Preparation of Graphene Quantum Dots from Pyrolyzed Alginate

ARTICLE *in* LANGMUIR · APRIL 2013

Impact Factor: 4.46 · DOI: 10.1021/la400618s · Source: PubMed

Langmuir

Article

pubs.acs.org/Langmuir

Preparation of Graphene Quantum Dots from Pyrolyzed Alginate

Pedro Atienzar,[†,§] Ana Primo,[†,§] Cristina Lavorato,[†,‡] Raffaele Molinari,[‡] and Hermenegildo García*[,†]

[†]Instituto Universitario de Tecnología Química CSIC-UPV, Univ. Politecnica de Valencia, Av. De los Naranjos s/n, 46022 Valencia, Spain

[‡]Department of Environmental and Chemical Engineering, University of Calabria, Via P. Bucci, 44/A, 87036 Rende, CS, Italy

ABSTRACT: Pyrolysis at 900 °C under an inert atmosphere of alginate, a natural widely available biopolymer, renders a graphitic carbon that upon ablation by exposure to a pulsed 532 nm laser (7 ns, 50 mJ pulse^{-1}) in acetonitrile, water, and other solvents leads to the formation of multilayer graphitic quantum dots. The dimensions and the number of layers of these graphitic nanoparticles decrease along the number of laser pulses from 100 to 10 nm average and from multiple layers to few layers graphene (1−1.5 nm thickness), respectively, leading to graphene quantum dots (GQDs). Accordingly, the emission intensity of these GQDs increases appearing at about 500 nm in the visible region along the reduction of the particle size. Transient absorption spectroscopy has allowed detection of a transient signal decaying in the microsecond time scale that has been attributed to the charge separation state.

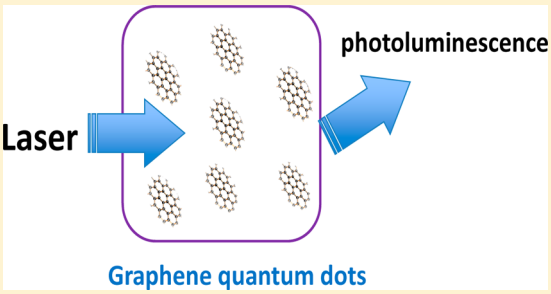

INTRODUCTION

Graphene (G) being one atom thick layer of extended sp^2 carbons represents the limit of the thinnest possible 2D conductive surface,[1,2] exhibiting very fast electron mobility and high charge carrier density.[3] One of the most convenient procedures for the preparation of G suspensions consists in the deep oxidation of graphite flakes followed by exfoliation of the resulting graphite oxide by sonication in the appropriate solvent and reconstitution of G by reduction of the dispersed graphene oxide (GO).[4−6] While this methodology enjoys high reproducibility and can produce highly concentrated aqueous suspensions of GO (about 0.1 mg L^{-1}), the materials present in the suspensions are typically constituted by micrometric sheets of nanometric thickness. Because of the remarkable properties derived from 2D confinement at the nanoscale caused by the effect of the edges, G *quantum dots* (GQDs) exhibit new properties such as emission and their behavior as spin qubit with collective spin states.[7,8] Recent reviews have summarized the unique properties of GQDs.[9−14] It is, therefore, very important to develop reliable and efficient procedures for the preparation of GQDs to exploit their unique properties arising from confinement. Unfortunately, graphite oxidation and exfoliation is not a suitable procedure to obtain GQDs, since it fails to provide nanometric sheets that have a large tendency to undergo complete oxidation to CO_2 and other alternative procedures have to be implemented. For this reason GQDs have to be prepared in alternative ways, such as for instance by acid-catalyzed microwave pyrolysis of carbon precursors.[15]

Because of their size, GQDs form persistent dispersions in different solvents and may have large biomedical application due to the possibility to cross cellular membranes.[16] Also, GQDs have attracted considerable attention as emerging fluorescent dots for bioimaging, sensing,[17] pollutant removal,[18] and even in photovoltaic devices.[19] GQDs also hold promise in catalysis due to their large surface area and accessibility of the active sites.[20] In the present work we report an innovative and efficient preparation of GQDs of tunable dimensions and describe the unique photophysical properties GQD suspensions.

RESULTS AND DISCUSSION

We have recently reported that pyrolysis of natural chitosan can form G films on various supports.[21] On the basis of this finding, we performed the pyrolysis of millimetric alginate beads at 900 °C to form graphitic carbon residues. XRD patterns of these alginate-derived carbons show that pyrolyzed alginate beads have a tendency to form graphitic carbons, although the broadness of the peak at 23° indicates low crystallinity and loose *z*-stacking compared to graphite (Figure 1). Similar observations that pyrolysis of alginate form graphitic carbons have been already reported in the literature.[22]

When carbon residues from alginate were submitted to ablation in a solvent using 532 nm laser pulses, an increasing darkening of the liquid phase is observed. Figure 2 shows the increasing intensity of the optical UV−vis absorption spectra of acetonitrile upon 532 nm laser ablation of the alginate derived carbon in contact with this solvent, suggesting that some carbon residue is detached from the submillimetric solid carbon beads, becoming suspended in the liquid phase. We noticed that the region 200−300 nm (not shown in Figure 2) contain some fine structure in the optical spectra that could correspond to the liberation of small condensed polycyclic aromatic

Received: February 16, 2013
Revised: April 18, 2013
Published: April 26, 2013

   dx.doi.org/10.1021/la400618s | *Langmuir* 2013, 29, 6141−6146

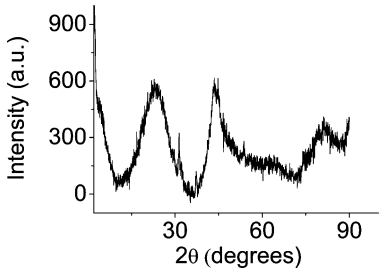

Figure 1. XRD pattern of the alginate derived carbon obtained by pyrolysis at 900 °C.

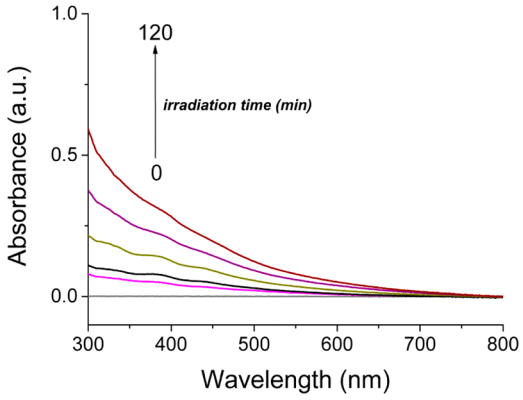

Figure 2. UV−vis spectra of acetonitrile in contact with alginate-derived carbon beads that has been submitted to ablation with 532 nm nanosecond laser pulses (1 Hz pulse frequency) for an increasing time (0, 30, 60, 90, and 120 min).

compounds during laser ablation. The 300−800 nm show an increasing absorption intensity of the liquid phase upon prolonging the laser treatment, indicating that the extent of graphitic debris in the solution increases over the time.

In related precedents it has been reported that λ_{max} depends on the size of the GQD. The fact that Figure 2 does not show these variations suggests that in the present case there is a polydispersity in the size distribution that does not allow to discriminate the average size by optical spectroscopy.[9]

The presence of G dispersed in acetonitrile was confirmed by Raman spectroscopy of the residue resulting after removing acetonitrile by evaporation where the presence of the two peaks corresponding to the G and D bands of graphene at 1600 and 1360 cm^{-1} was observed (Figure 3a). The large intensity of the D band observed in Figure 3a could be related to the presence of defects associated with the small particle size and the relative large contribution of functional groups in the periphery of the particles. XP spectroscopy can monitor the energy of the core electrons of the elements present in the carbon residue. The XP spectra of the material resulting after laser ablation are also compatible with the presence of G in the acetonitrile dispersion, showing the C 1s peak characteristic of G (Figure 3b). Deconvolution of the experimental C 1s peak suggests the presence of two components at 284.8 and 287.4 eV binding energies that are compatible with the assignment to graphitic and carboxylic carbons, respectively. The large proportion of carboxylic carbons (∼15%) in comparison with other G samples suggests the small dimension of the G residue, being compatible with a large ratio between periphery and internal carbons as observed in microscopy.

AFM and TEM images of the carbon residue present in acetonitrile after laser ablation were crucial to show the presence of GQD flakes with small dimensions. The average number of layers of the GQD and the dimensions of the flakes decrease along the number of laser pulses, suggesting that the initial suspended graphitic debris of small dimensions is undergoing further exfoliation in acetonitrile. While the nanoparticles present at initial stages of the ablation process can be better considered as graphitic quantum dots, the decrease in the number of layers upon increasing the number of laser shots leads to few-layers GQDs. In fact, the graphitic debris present at shorter laser ablation treatments exhibits a larger dispersion in sizes and number of layers, while as the ablation time increases the colloidal particles tend to be GQDs of narrower particle size. Figure 4 shows illustrative AFM images of the type of material present in acetonitrile solution by ablation of the alginate-derived carbons as a function of the photolysis time. Thus, graphitic debris at 5 min of laser exposure consisted in particles of about 100 nm length and from 5 to 30 nm thickness, corresponding to multilayer G flakes. At 40 min ablation, acetonitrile contained mostly GQDs of 10−20 nm length with 1−1.5 nm depth on average corresponding to single or few layer GQDs. A rough estimation of an apparent quantum yield of GQD formation based on the 60 min irradiation at 10 Hz assuming the complete exfoliation of 1.5 mg of precursor indicates that each pulse forms about 10^{10} GQD considering an average 20 nm size. Electron diffraction of the material present in acetonitrile shows the polycrystalline nature of the sample indicating that the suspended carbon residue corresponds to small particles of well-defined G layers (Figure 5a). TEM image shows the

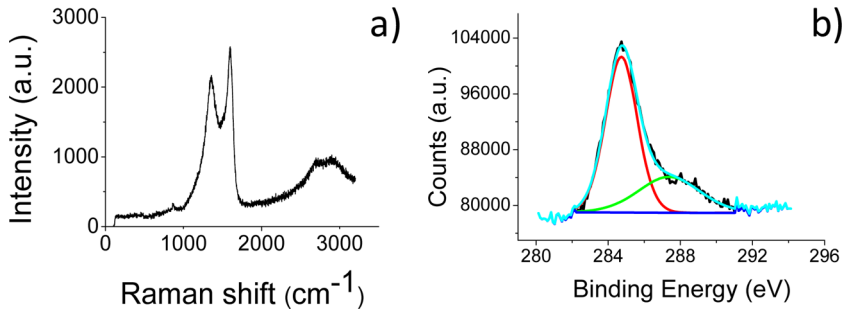

Figure 3. (a) Raman spectra and (b) C 1s XPS peak of the alginate derived carbon after pyrolysis at 900 °C. Note in Raman spectra the presence of the 2D band in the region between 2500 and 2900 cm^{-1} that is characteristic of highly crystalline G samples, while the presence of the 1360 cm^{-1} is associated with the large proportion of peripheral carbons. The experimental C 1s peak has been fitted to two components of binding energies 284.8 and 287.4 eV, respectively.

dx.doi.org/10.1021/la400618s | *Langmuir* 2013, 29, 6141−6146

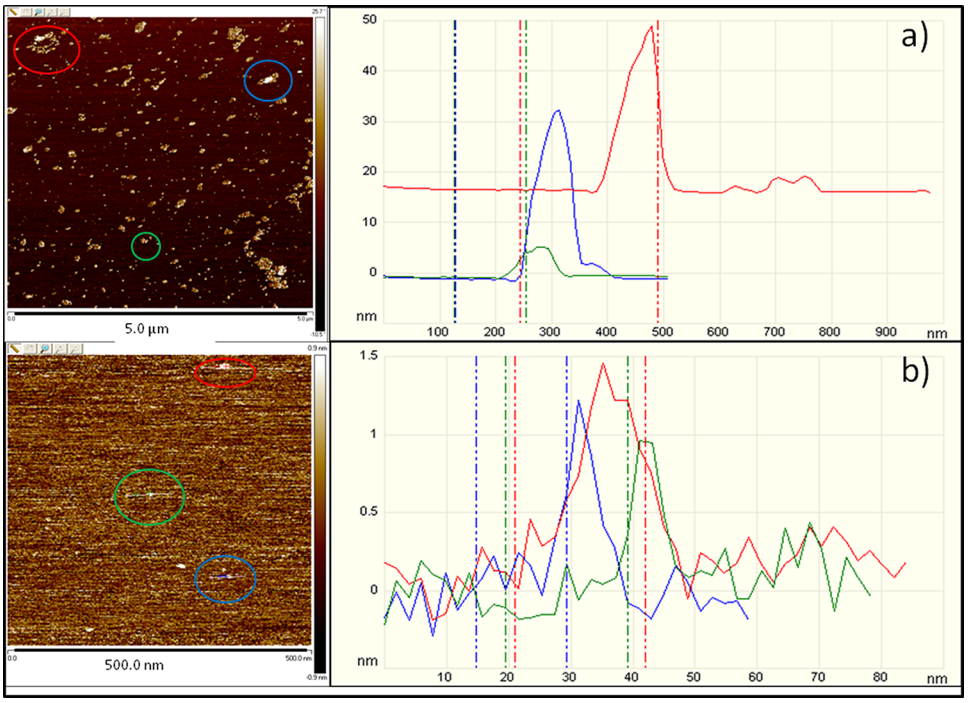

Figure 4. AFM images (left) and corresponding height profile (right) measured for the GQD flakes present in acetonitrile suspension after 5 min (a) and 40 min (b) ablation time. The circles indicate the particles whose heights have been measured in the right. Each particle has been identified by the same color in the left and right side.

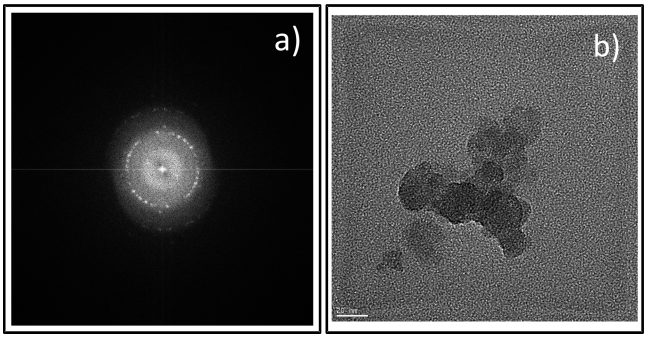

Figure 5. Electron diffraction (a) and high-resolution TEM image (b) of the GQD dissolved in acetonitrile after 532 nm laser ablation for 40 min.

expected morphology for the GQD material present in acetonitrile (Figure 5b). The information provided in Figure 5 is crucial to firmly support that the carbon debris present in the liquid phase after laser ablation is crystalline and has the structure of G, although its dimensions are small.

The same behavior commented for acetonitrile was also observed when the laser ablation was performed using water and ethanol as solvents, indicating that the procedure appears general for the preparation of persistent dispersions of GQDs in a liquid phase. Moreover, no influence of the suspension temperature was observed, and identical results in terms of variation of the optical spectrum were observed when the laser ablation was carried out at 60 °C.

On the basis of the reported formation of G by pyrolysis of alginate,[22] the graphitic nature of the alginate-derived carbon residues, and the previous reports on the literature about

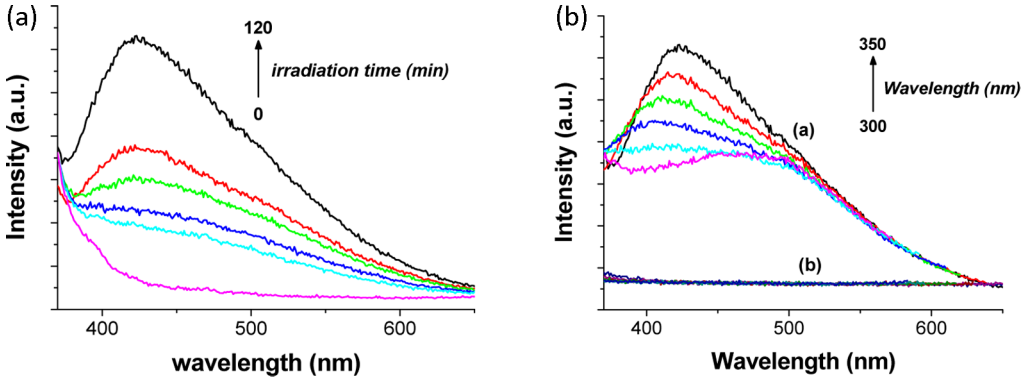

Figure 6. (a) Fluorescence spectra of acetonitrile solutions of GQDs after excitation at 350 nm obtained from pyrolyzed alginate upon increasing the laser exposure for 0, 5, 10, 20, 40, and 120 min. (b) Fluorescence spectra (plots (a)) of an acetonitrile solution of GQD after irradiation for 120 min as a function of the excitation wavelength from 300 to 350 nm every 10 nm. Plots (b) correspond to the emission of the pyrolysed alginate precursors not submitted to laser ablation.

dx.doi.org/10.1021/la400618s | *Langmuir* 2013, 29, 6141−6146

graphite exfoliation by laser ablation,[23] we propose that, in the present case, laser ablation is causing exfoliation of graphitic debris from submillimetric pyrolyzed alginate beads in the form of small GQDs that become easily suspended in the liquid phase. Considering that alginate is a biomass waste, the present finding constitutes a remarkable example of biomass valorization by transforming this waste into a material of high added value.

It has been reported that GQDs can exhibit blue emission,[24−26] although the intensity of the emission increases upon surface passivation by appropriate functionalization with poly(ethylene glycol) or suitable groups.[27,28] In the present case, we have observed that the GQDs prepared by laser ablation from pyrolyzed alginate also emit. Since the emission intensity in water can be somewhat lower due to some quenching, acetonitrile was selected to determine the photoluminescence properties of GQDs prepared here. In contrast, G sheets obtained by sonication of pyrolyzed alginate beads do not exhibit any emission even in acetonitrile. The key features of the emission are that (i) the emission maximum depends, particularly for larger GQD particles, on the excitation wavelength and (ii) there is a notable influence of the size and ablation time on the emission that increases in intensity as the GQD size decreases. The first feature can be interpreted as indicating a large inhomogeneity in the GQD samples that at initial times would be constituted by a range of graphitic debris, each particular quantum dot being excited preferentially at a particular wavelength. The second property, i.e., the increase of photoluminescence intensity with the ablation time, can be related to the decrease in the average size of the GQD, since photoluminescence is an intrinsic property of small G sheets. Figure 6 illustrates these two emission features that are indicative of the quantum confinement of the exciton, the most emissive GQD sample being the one obtained at the longest ablation time that exhibits a fluorescence peak at 430 nm after excitation at 350 nm. Worth noting is that some of the samples whose photoluminescence is shown in Figure 6 are the same than those whose absorption spectra are presented in Figure 2. Excitation spectra of the emission monitoring at wavelengths in the range of 390−510 nm for the GQD sample prepared at the longest ablation time are shown in Figure 7. As can be seen there, the excitation spectra vary with the emission wavelength, indicating that photoluminescence peaks arise from different emitting species. It is worth noting that Figures 2 and 6 can be used to follow in a simple way the progress of the formation of GQDs from pyrolyzed alginate beads and the decrease in the particle size.

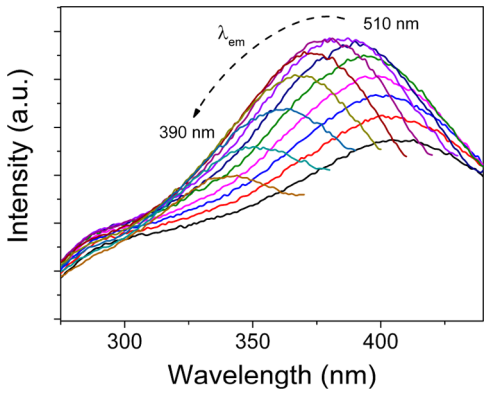

Figure 7. Excitation spectra monitoring different emission wavelengths (indicated in the plot) recorded for an acetonitrile solution of GQDs obtained after 120 min ablation time.

Typically, the emission intensity in GQDs should change with the average particle size. The fact that no much variation in the position of the λ_{em} is observed as a function of the ablation time could be again related to the polydispersity of the GQDs. Nevertheless, we performed the corresponding excitation spectra at different emission wavelengths for samples after the longest ablation time. Figure 7 presents these spectra. A clear red-shift in the position of λ_{ex} as a function of the emission wavelength provides support to the distribution of the particle size observed by imaging techniques.

To gain understanding on the photophysics of the GQDs prepared in the present study, the samples were also studied by transient absorption spectroscopy. 532 nm excitation of a GQD solution in acetonitrile allows the detection of a transient spectrum characterized by a continuous absorption in the entire monitored wavelength range (Figure 8). The temporal profile

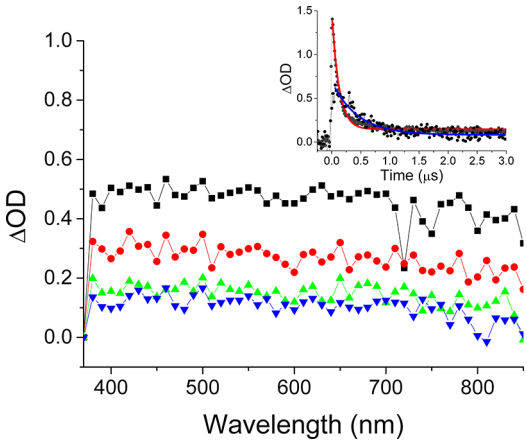

Figure 8. Transient spectra recorded at 0.21 (■), 0.61 (●), 1.01 (▲), and 1.41 μs (▼) after 532 nm laser excitation of an Ar-purged acetonitrile solution of GQD. The inset shows the signal decay monitored at 500 nm of an Ar-purged solution.

of the signals was coincident at all wavelengths, suggesting that these spectra correspond to a single species (inset of Figure 8). The signal decay shows two regimes, one of them decaying faster in less than 1 μs, followed by a slower decay taking place in tens of microseconds. The relative contribution of these two regimes can be estimated from the relative intensity of the signals immediately after the laser pulse and after 1 μs as 80 and 20%, respectively.

On the basis of the precedents reported in the literature about this continuous transient absorption,[29] we attribute this species to a charge separation state with the generation of electrons in the upper conduction band and positive holes in the occupied molecular orbitals of the highest energies. In support of this assignment, the signal intensity grows upon addition of methanol and decreases upon oxygen quenching. The temporal profile would be indicative of, at least, two main deactivation mechanisms, probably by recombination of geminate electrons and holes (fast decay) or annihilation after migration of the charges away from the initial point of charge separation and subsequent recombination after random walk. It should be, however, commented that controls submitting to transient spectroscopy analogous suspensions of

dx.doi.org/10.1021/la400618s | Langmuir 2013, 29, 6141−6146

G sheets obtained by exfoliation of pyrolyzed alginate beads also exhibit similar transient spectra, although lacking the shortest component of the signal and reaching lower intensity. Therefore, it seems that these microsecond transients attributable to charge separation are not specific of GQDs and should not be responsible for the emission that could probably arise from much shorter lived species. In fact, the emission lifetime of the GQDs (estimated by fitting the temporal profile to a single-exponential decay) varies somewhat depending on the monitored emission wavelength in the range of 390−510 nm, being relatively independent of the ablation time (see inset of Figure 9). This emission varies in the range of

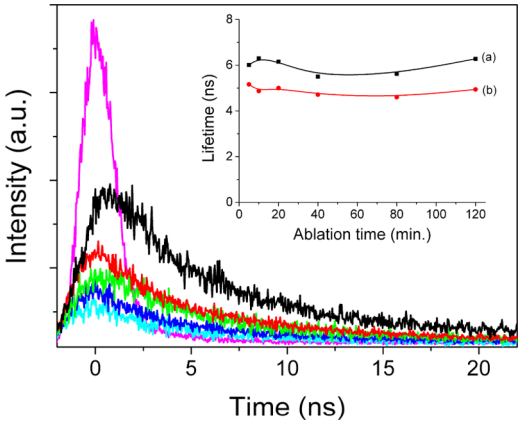

Figure 9. Temporal profile of the emission monitored at 500 nm upon 350 nm excitation for a series of GQDs. The profiles correspond (from top to bottom) to the samples obtained after 5 (cyan), 10 (blue) 20 (green), 40 (red), and 120 min (black) laser ablation treatment. The shortest pink plot corresponds to the profile of the lamp. The decrease in emission intensity should be attributed to the shift in the λ_{ex} excitation wavelength as observed in Figure 6. Inset: emission lifetime estimated from the best fitting to a monoexponential decay of the emission signal monitored at 500 (a) or 430 (b) nm.

5−10 ns that should overlap, but it does not coincide, with the shortest regime observed in laser flash photolysis. Thus, although the system is very complex due to the polydispersity of the sample, it is clear that emissive species can only be present in the first microsecond after the laser pulse.

CONCLUSIONS

In summary, due to the loose packing of the graphitic carbon material resulting upon pyrolysis of alginate particles, as indicated by the broad XRD peaks, laser ablation in acetonitrile, water, or other solvents results in the leaching of small carbon debris from the solid to the solution. The process can be followed by different spectroscopic and imaging techniques that show that the amount of leached carbon debris increases upon laser exposure and that the morphology of these residues tends to GQDs by reducing the dimensions of the sheets and by increasing exfoliation. The resulting GQDs exhibit photoluminescence as a function of the ablation time, increasing in intensity as the ablation time increases. Thus, our study shows a convenient protocol to obtain GQDs from pyrolyzed alginate allowing a certain control on the size and properties of these nanoparticles.

EXPERIMENTAL SECTION

Synthesis of Graphene (G) Quantum Dots: Alginic acid sodium salt beads from brown algae (commercially available from Sigma) were pyrolyzed in argon atmosphere using the following oven program: 200 °C during 2 h for annealing and then heating at 10 °C/min up to 900 °C for 6 h. This multilayer graphitic powder is stirred magnetically in water or acetonitrile in a quartz cuvette and exposed to the pulses from the second harmonic of a Nd:YAG laser (50−130 mJ pulse^{-1}). The suspension becomes increasing black as the time of the laser ablation increases. After the treatment, the supernatant was collected by decantation and characterized by UV−vis optical spectroscopy using a Cary 5G spectrophotometer. Raman spectra were recorded after solvent evaporation by casting a drop of the suspension on a glass substrate. XRD patterns of the pyrolyzed alginate beads were recorded by milling the beads and compressing the powder in the corresponding sample holder. XRD patterns were recorded on a Philips Cubix Pro using Cu Kα radiation at 45 kV and 40 mA in the 2θ range from 5° to 70°.

Textural and Analytical Properties Measurements: Raman spectra were recorded at ambient temperature with 514 nm laser excitation by using a Renishaw In Via Raman spectrometer equipped with a CCD detector.

TEM images were recorded in a Philips CM300 FEG system with an operating voltage of 100 kV. XPS spectra were recorded on a SPECS spectrometer equipped with a Phoibos 150 9MCD detector using a nonmonochromatic X-ray source (Al and Mg) operating at 200 W. The samples were evacuated in the prechamber of the spectrometer at 1 × 10^{-9} mbar. Some of the samples have been activated in situ in nitrogen flow at 450 °C for 3 h followed by evacuation at 10^{-8} mbar. The measured intensity ratio of components was obtained from the area of the corresponding peaks after nonlinear Shirley-type background subtraction and corrected by the transmission function of the spectrometer. The atomic force microscopic measurements were conducted using contact mode in air at ambient temperature using a Veeco AFM apparatus. Laser ablation was carried out using a second-harmonic output of Nd:YAG laser from Spectra Physics operating a 1 Hz. The pyrolyzed alginate beads were placed in a septum-capped 1 × 1 cm^2 quartz cuvette that was magnetically stirred while abladed. After the required time, an aliquot of the suspension (100 μL) was filtered and analyzed by optical spectroscopy. Emission and excitation spectra were recorded in a PTI spectrofluorimeter having Czerny Turner monochromators. Transient spectra were recorded using a Luzchem laser flash photolysis apparatus. The experiment was controlled by a computer that controlled data acquisition and provided data storage capability. The samples were submitted to N_2 purging at least 15 min before the experiments.

AUTHOR INFORMATION

Corresponding Author

*E-mail: hgarcia@qim.upv.es (H.G.).

Author Contributions

§P.A. and A.P. have contributed equally to this work.

Notes

The authors declare no competing financial interest.

ACKNOWLEDGMENTS

Financial support by the Spanish MINECO (Severo Ochoa and CTQ2012-32315) is gratefully acknowledged. C.L. thanks the European Commission, the European Social Fund, and the Regione Calabria for a postgraduate scholarship and funding for her stay in Valencia.

REFERENCES

(1) Geim, A. K.; Novoselov, K. S. The rise of graphene. *Nat. Mater.* **2007**, *6*, 183−191.

(2) Novoselov, K. S.; Geim, A. K.; Morozov, S. V.; Jiang, D.; Zhang, Y.; Dubonos, S. V.; Grigorieva, I. V.; Firsov, A. A. Electric field effect in atomically thin carbon films. *Science* **2004**, *306*, 666−669.
(3) Bolotin, K. I.; Sikes, K. J.; Jiang, Z.; Klima, M.; Fudenberg, G.; Hone, J.; Kim, P.; Stormer, H. L. Ultrahigh electron mobility in suspended graphene. *Solid State Commun.* **2008**, *146*, 351−355.
(4) Park, S.; Ruoff, R. S. Chemical methods for the production of graphenes. *Nat. Nanotechnol.* **2009**, *4*, 217−224.
(5) Stankovich, S.; Dikin, D. A.; Piner, R. D.; Kohlhaas, K. A.; Kleinhammes, A.; Jia, Y.; Wu, Y.; Nguyen, S. T.; Ruoff, R. S. Synthesis of graphene-based nanosheets via chemical reduction of exfoliated graphite oxide. *Carbon* **2007**, *45*, 1558−1565.
(6) Zhu, Y. W.; Murali, S.; Cai, W. W.; Li, X. S.; Suk, J. W.; Potts, J. R.; Ruoff, R. S. Graphene and graphene oxide: Synthesis, properties, and applications. *Adv. Mater.* **2010**, *22*, 3906−3924.
(7) Ponomarenko, L. A.; Schedin, F.; Katsnelson, M. I.; Yang, R.; Hill, E. W.; Novoselov, K. S.; Geim, A. K. Chaotic Dirac billiard in graphene quantum dots. *Science* **2008**, *320*, 356−358.
(8) Trauzettel, B.; Bulaev, D. V.; Loss, D.; Burkard, G. Spin qubits in graphene quantum dots. *Nat. Phys.* **2007**, *3*, 192−196.
(9) Baker, S. N.; Baker, G. A. Luminescent carbon nanodots: Emergent nanolights. *Angew. Chem., Int. Ed.* **2010**, *49* (38), 6726−6744.
(10) Cao, L.; Meziani, M. J.; Sahu, S.; Sun, Y. P. Photoluminescence properties of graphene versus other carbon nanomaterials. *Acc. Chem. Res.* **2013**, *46* (1), 171−180.
(11) Jiang, H. J. Chemical preparation of graphene-based nanomaterials and their applications in chemical and biological sensors. *Small* **2011**, *7* (17), 2413−2427.
(12) Recher, P.; Trauzettel, B. Quantum dots and spin qubits in graphene. *Nanotechnology* **2010**, *21* (30).
(13) Rozhkov, A. V.; Giavaras, G.; Bliokh, Y. P.; Freilikher, V.; Nori, F. Electronic properties of mesoscopic graphene structures: Charge confinement and control of spin and charge transport. *Phys. Rep.* **2011**, *503* (2−3), 77−114.
(14) Sheng, W. D.; Korkusinski, M.; Guclu, A. D.; Zielinski, M.; Potasz, P.; Kadantsev, E. S.; Voznyy, O.; Hawrylak, P. Electronic and optical properties of semiconductor and graphene quantum dots. *Front. Phys.* **2012**, *7* (3), 328−352.
(15) Liu, S.; Wang, L.; Tian, J.; Zhai, J.; Luo, Y.; Lu, W.; Sun, X. Acid-driven, microwave-assisted production of photoluminescent carbon nitride dots from N,N-dimethylformamide. *RSC Adv.* **2011**, *1* (6), 951−953.
(16) Markovic, Z. M.; Ristic, B. Z.; Arsikin, K. M.; Klisic, D. G.; Harhaji-Trajkovic, L. M.; Todorovic-Markovic, B. M.; Kepic, D. P.; Kravic-Stevovic, T. K.; Jovanovic, S. P.; Milenkovic, M. M.; Milivojevic, D. D.; Bumbasirevic, V. Z.; Dramicanin, M. D.; Trajkovic, V. S. Graphene quantum dots as autophagy-inducing photodynamic agents. *Biomaterials* **2012**, *33*, 7084−7092.
(17) Lu, W.; Qin, X.; Liu, S.; Chang, G.; Zhang, Y.; Luo, Y.; Asiri, A. M.; Al-Youbi, A. O.; Sun, X. Economical, green synthesis of fluorescent carbon nanoparticles and their use as probes for sensitive and selective detection of mercury(II) Ions. *Anal. Chem.* **2012**, *84* (12), 5351−5357.
(18) Liu, S.; Tian, J.; Wang, L.; Zhang, Y.; Luo, Y.; Asiri, A. M.; Al-Youbi, A. O.; Sun, X. A novel acid-driven, microwave-assisted, one-pot strategy toward rapid production of graphitic N-doped carbon nanoparticles-decorated carbon flakes from N,N-dimethylformamide and their application in removal of dye from water. *RSC Adv.* **2012**, *2* (11), 4632−4635.
(19) Shen, J.; Zhu, Y.; Yang, X.; Li, C. Graphene quantum dots: emergent nanolights for bioimaging, sensors, catalysis and photovoltaic devices. *Chem. Commun.* **2012**, *48*, 3686−3699.
(20) Liu, S.; Tian, J.; Wang, L.; Luo, Y.; Sun, X. A general strategy for the production of photoluminescent carbon nitride dots from organic amines and their application as novel peroxidase-like catalysts for colorimetric detection of H_2O_2 and glucose. *RSC Adv.* **2012**, *2* (2), 411−413.
(21) Primo, A.; Atienzar, P.; Sánchez, E.; Delgado, J. M.; García, H. From biomass wastes to large-area, high-quality, N-doped graphene: catalyst-free carbonization of chitosan coatings on arbitrary substrates. *Chem. Commun.* **2012**, *48*, 9254−9256.
(22) Primo, A.; Forneli, A.; Corma, A.; García, H. From biomass wastes to highly efficient CO_2 adsorbents: Graphitisation of chitosan and alginate biopolymers. *ChemSusChem* **2012**, *5*, 2207−2214.
(23) Qian, M.; Zhou, Y. S.; Gao, Y.; Feng, T.; Sun, Z.; Jiang, L.; Lu, Y. F. Production of few-layer graphene through liquid-phase pulsed laser exfoliation of highly ordered pyrolytic graphite. *Appl. Surf. Sci.* **2012**, *258*, 9092−9095.
(24) Shen, J. H.; Zhu, Y. H.; Chen, C.; Yang, X. L.; Li, C. Z. One-pot green synthesis of optically pH-sensitive carbon dots with upconversion luminescence. *Chem. Commun.* **2010**, *47*, 2580−2582.
(25) Silva, A. M.; Pires, M. S.; Freire, V. N.; Albuquerque, E. L.; Azevedo, D. L.; Caetano, E. W. S. Graphene nanoflakes: Thermal stability, infrared signatures, and potential applications in the field of spintronics and optical nanodevice. *J. Phys. Chem. C* **2011**, *114*, 17472−17485.
(26) Wang, Q. L.; Zheng, H. Z.; Long, Y. J.; Zhang, L. Y.; Gao, M.; Bai, W. J. Microwave−hydrothermal synthesis of fluorescent carbon dots from graphite oxide. *Carbon* **2012**, *49*, 3134−3140.
(27) Shen, J. H.; Zhu, Y. H.; Yang, X. L.; Zong, J.; Zhang, J. M.; Li, C. Z. One-pot hydrothermal synthesis of graphene quantum dots surface-passivated by polyethylene glycol and their photoelectric conversion under near-infrared light. *New J. Chem.* **2012**, *36*, 97−101.
(28) Tang, L. B.; Ji, R. B.; Cao, X. K.; Lin, J. Y.; Jiang, H. X.; Li, X. M.; Teng, K. S.; Luk, C. M.; Zeng, S. J.; Hao, J. H.; Lau, S. P. Deep ultraviolet photoluminescence of water-soluble self-passivated graphene quantum dots. *ACS Nano* **2012**, *6*, 5102−5110.
(29) de Miguel, M.; Álvaro, M.; García, H. Graphene as a quencher of electronic excited states of photochemical probes. *Langmuir* **2012**, *28*, 2849−2857.